Exploratory Study of a Millimeter Resonance Isolator for the Circular Electric Waveguide Mode

R. A. HENSCHKE, SENIOR MEMBER, IEEE

Summary—A feasibility study was made on a TE_{01} mode circular waveguide resonance isolator at frequencies near 35 Gc. A design was developed which utilized circumferentially oriented and magnetized thin rings of hexagonal ferrite material in contact with the inner or outer surface of a ring of alumina ceramic mounted concentrically in the waveguide. Approximate experimental measurements indicated that appreciable nonreciprocal attenuation could be obtained without severe degradation of the mode purity. Expressions are given for the field distributions in the dielectric ring loaded wave guide and for the ellipticity of the magnetic fields at the surfaces of the ring. Magnetic field ellipticity is computed as a function of a "slow-wave mode" cutoff constant for an experimental ring configuration. For sufficiently large values of this constant, the magnetic fields at the boundary are almost circularly polarized and are relatively independent of mean ring radius. The analytical results tend to support the experimental findings.

I. Introduction

IT IS WELL KNOWN that energy can be transmitted in the TE_{01} circular waveguide mode with very low attenuation per unit length and at very high peak power levels. Furthermore, under optimum transmission conditions, the energy loss per unit length for this mode is less than that for more conventional modes of propagation. For this reason, the circular electric mode has long been of interest for millimeter wave transmission applications. Other applications may follow as a result of the recent development of high power millimeter wave tubes which convert energy directly to this mode. The development of standard TE_{01} circular waveguide components is therefore a matter of some practical interest. This paper is a report of the experimental and analytical findings of a feasibility study of a TE_{01} mode resonance isolator at frequencies near 35 Gc. Although the isolator which evolved from this study did not meet exacting stands for attenuation and mode purity, the study indicated feasibility and provided useful design information.

A basic design for a ferrite resonance isolator operating in the TE_{01} circular waveguide mode has been given by Fox, Miller and Weiss [1]. The design which they suggest utilizes a thin, circumferentially magnetized, ferrite ring located concentrically in the circular waveguide and having a radius for which the RF magnetic fields in the ferrite are almost circularly polarized in a plane normal to the direction of magnetization.

Manuscript received March 6, 1964. The work described here was carried out at Melabs, Palo Alto, Calif., and was supported under Signal Corps Contract No. DA 35-039-SC-88949.

The author is with the Microwave Physics Department, Fairchild Semiconductor, Palo Alto, Calif. He was formerly with Melabs, Palo Alto, Calif.

There are serious practical problems associated with resonant ring configurations.

1) The ferrite must be circumferentially magnetized with a very strong dc magnetic field, but there is no practical way of applying this field internally.
2) The basic mode of propagation is a higher order mode which may readily convert to other modes at an asymmetric discontinuity or obstacle. Thus, the maintenance of mode purity may be difficult.

The first problem has been overcome through the development of oriented hexagonal, ferrite materials capable of providing high internal anisotropy fields in the direction of crystal orientation. It was found that circumferentially oriented ferrite rings could be fabricated with an internal, circumferential anisotropy field of approximately 11,500 oersteds,[1] so that they were capable of resonance at 35 Gc.

It was difficult to estimate the magnitude of the mode purity problem. The number of possible propagating modes was restricted to ten by using a waveguide diameter of 0.634 inch over an operating frequency range of 33–37 Gc. Higher order TE_{0n} modes were cut off in the empty waveguide. However, there was a possibility of exciting them in the section of waveguide containing the ferrite ring. It was felt that the circular symmetry of the ferrite ring would prevent excitation of circularly asymmetric modes, but that these might be excited to some extent by misalignment of the rings. Ultimately, the utility of the design could only be determined by experimentation.

II. Design Approach

The theory of operation of ferrite resonance isolators has been discussed by a number of authors [1], [2]. In designing for practical applications, one attempts to locate a small ferrite element inside a transmission line or waveguide in a region where the RF magnetic fields are circularly polarized, with the sense of circular polarization dependent on the direction of propagation. When the ferrite is magnetized to resonance in a direction normal to the plane of circular polarization, it interacts strongly with the RF fields for propagation in one direction, but does not interact with energy propagating in the opposite direction. One generally computes the location of the region of circular polarization for

[1] Fabricated for USAERDL by North American Philips Labs., Irvington-on-Hudson, N. Y., under Contract DA36-039 SC-85279; July, 1950–July, 1961.

the unperturbed transmission structure, locates the ferrite in this region and then proceeds to optimize the design by "cut and try" methods. This procedure is generally useful in constructing isolators for any transmission structure and may be applied to the design under consideration here.

Basic design computations are readily carried out for the configuration described by Fox, Miller and Weiss [1]. The RF magnetic fields in TE_{01} circular waveguide have radial and longitudinal components in phase quadrature. The circularly polarized regions are found by determining radii for which the magnitudes of these components are equal. These regions are infinitely thin cylinders having either of two radii obtained as a solution of

$$\frac{J_1^2(k_c r)}{J_0^2(k_c r)} = \frac{1}{k_0^2/k_c^2 - 1}, \tag{1}$$

where $J_0(k_c r)$ and $J_1(k_c r)$ are zero and first-order Bessel functions of argument $k_c r$. The constants are $k_c = 3.8317/a$, a constant related to the waveguide cutoff frequency; $k_0 = \omega\sqrt{\mu_0\epsilon_0} = 2\pi/\lambda_0$, the free space propagation constant; λ_0 = free space wavelength; a = guide radius. For a waveguide of radius 0.317 inch, the radii of circular polarization at 35 Gc are approximately 0.109 inch and 0.263 inch. The radii calculated from (1) are sensitive functions of frequency. For this reason the Fox, Miller and Weiss configuration should operate satisfactorily over relatively narrow bandwidths. To devise a broad-band configuration for the circular electric mode, it is instructive to consider a broad-band configuration used in TE_{10} mode rectangular waveguide. Reasoning by analogy, we may arrive at an appropriate TE_{01} circular waveguide configuration.

A broad-band resonance isolator may be constructed in TE_{10} mode rectangular waveguide loaded by a thin dielectric slab of relatively high permittivity, extending completely across its narrow dimension and located laterally near the waveguide center line [3]. The dielectric slab tends to confine the circularly polarized region at, or very near, its surface for a wide range of frequencies [4]. An isolator may be constructed by placing a thin ferrite slab adjacent to the dielectric slab and magnetizing it in a direction normal to the broad wall of the waveguide. The attenuation of the isolator is then primarily a function of the ferrite magnetization and linewidth but not of its location. Optimum concentration of the RF field in the ferrite region is obtained by experimentally adjusting the location and thickness of the dielectric slab.

The circular waveguide analog of this design consists of a concentrically mounted dielectric ring having a circumferentially magnetized ferrite ring at its inner or outer surface. It was felt that the circular symmetry of such a structure would prevent the excitation of many undesirable modes. However, it was not clear whether higher order TE_{0n} modes, which were capable of propagating in the dielectric loaded region, would seriously affect the design. It was decided that initial effort should be of an exploratory and experimental nature to determine general feasibility. If the exploratory measurements were promising, some attempt could be made to arrive at an improved design by analytical methods in order to conserve the limited supply of ferrite rings.

III. Exploratory Measurements

The orieuted ferrite rings, fabricated by North American Philips Laboratories, had wall thicknesses of approximately 0.050 inch and mean radii approaching the values of 0.109 inch and 0.263 inch computed as solutions of (1). It had been intended that these rings would be ground to a very thin wall and used as an approximation to the configuration suggested by Fox, Miller and Weiss [1]. However, it did not appear mechanically possible to grind the small rings to a wall thickness of less than 0.010 inch.

Exploratory measurements indicated that thin ferrite rings (wall thickness 0.010 inch), mounted carefully and concentrically with polyfoam supports, did not disturb the mode purity to a great extent and did provide nonreciprocal attenuation. This prompted further investigation, which involved dielectric loading of the ferrite rings using alumina ceramic ($\epsilon = 9.5$). Measurements indicated that the nonreciprocal attenuation characteristics of the magnetized ferrite rings were indeed enhanced when they were surrounded by a dielectric cylinder. However, development of a useful isolator required a reduction in the ferrite ring wall thickness [5].

For this purpose, the dielectric loading, which had proved to be electrically desirable, was also mechanically advantageous. When a small ferrite ring was bonded to the inside of a ceramic cylinder it was possible to grind the ferrite to a wall thickness of 0.004 inch. The dimensions of this ceramic and ferrite configuration are shown in Fig. 1(a). In order to determine the effect of variations in dielectric wall thickness. additional ceramic cylinders were ground so that they could be slipped over the first cylinder as in Fig. 1(b), thereby increasing the total wall thickness. Attenuation measurements for three different dielectric wall thicknesses are given in Fig. 2. The measurement techniques, as described in Appendix I, use an averaging process for determining the approximate attenuation. It will be noted that a fairly appreciable attenuation peak occurred in the forward direction near 34–34.5 Gc and above 36 Gc when a wall thickness of 0.035 inch was utilized. As the wall thickness was increased, these peaks appeared to shift out of the band of interest. To test the precision of the measurements a completely independent recheck was made on the same isolator elements at a later date.[2] In general, the repeated measurements followed the original measurements quite closely, although, in the case of the 0.035 inch dielectric wall, some deviation was

[2] Unpublished status report.

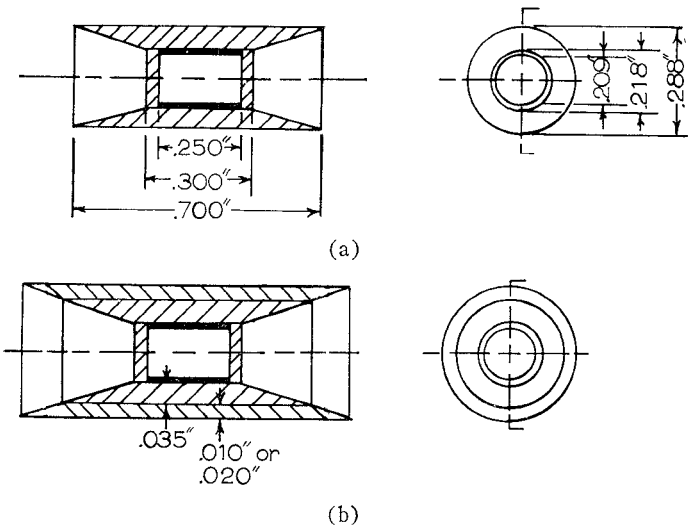

Fig. 1—(a) Ferrite ring mounted inside of ceramic cylinder having wall thickness of 0.035 inch. Cylinder wall tapered at each end for matching. (b) Configuration of (a) with additional ceramic sleeve used to increase the cylinder wall thickness. Isolators were constructed by mounting these configurations concentrically in circular waveguide using polystyrene foam supports.

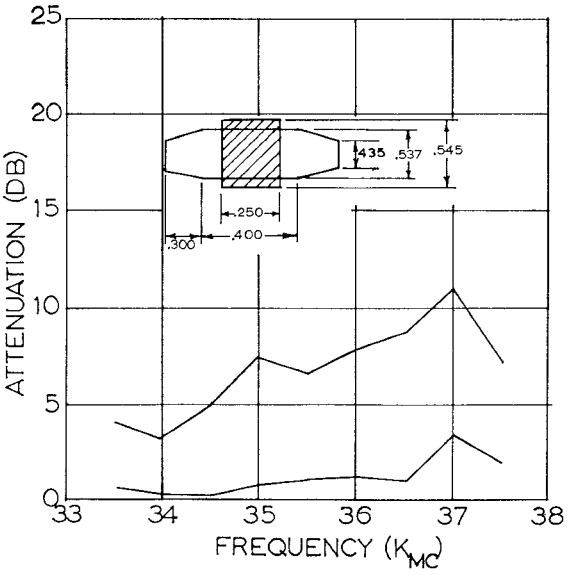

Fig. 3—Forward and reverse attenuation as a function of frequency for ferrite ring of 0.545-inch OD bonded to outside of 0.537-inch OD ceramic cylinder having 0.055-inch wall thickness and tapered ends.

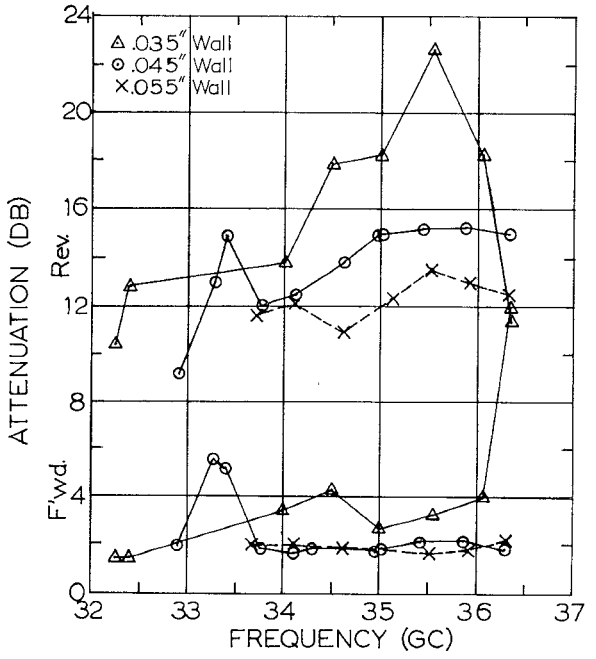

Fig. 2—Forward and reverse attenuation of configurations in Fig. 1(a) and (b) as a function of frequency.

noted in the vicinity of the forward attenuation peak near 34 Gc.

One of the large ferrite rings also was tested.[2] The measured forward and reverse attenuation are plotted in Fig. 3. Note that, for this ring, maximum attenuation occurs near 37 Gc, indicating that the anisotropy field may be slightly higher than it was in the smaller ferrite rings.

An indication of the mode purity also was obtained during measurements of power level. The definition for mode purity used here is: The ratio in decibels of the power propagating in the TE_{01} mode to the power propagating in an unwanted mode. An average power level in the waveguide may be obtained, as indicated in Appendix I, by averaging the maximum and minimum values of the circumferential variation of energy coupled to an external detector through a small hole in the circular waveguide wall. The magnitude of this variation provides a measure of the ratio of the unwanted signal at the coupling hole to the TE_{01} mode signal. As noted in Appendix I, a 1-db angular variation corresponds to a TE_{11} mode impurity about 20 db below the TE_{01} mode output. A 3-db variation corresponds to a TE_{11} mode impurity roughly 15 db down.

The attenuation measurements of Fig. 2 were made using mode filters between the ferrite loaded section and the coupling hole to improve measurement accuracy. The maximum angular variation noted for the configurations of Fig. 1 at any of the test frequencies, when these filters were used, was of the order of 3 db in the direction of small attenuation. (See Henschke [6]). Thus a minimum (most pessimistic) mode purity of about 15 db is indicated. Similar techniques were used in the measurements of Fig. 3, the angular variations for this case being of a generally comparable order of magnitude. The fact that the forward attenuations shown in Figs. 2 and 3 are fairly low at most frequencies is further indication of reasonably high mode purity. Excessive mode conversion should result in high energy loss in the filters and thus in large forward attenuation. The angular variation measured in the direction of reverse attenuation was generally larger than in the forward direction. Reasons for this difference in angular variation for the forward and reverse attenuation directions are given in Appendix I, together with additional measurement details.

While the data plotted in Figs. 2 and 3 are approximate, the exploratory measurements were felt to have established the fact that significant nonreciprocal attenuation was obtainable from the configurations of Figs. 1 and 3. Furthermore, the observed angular variations in the transmitted signal indicated that the mode purity was not severely degraded in the direction of forward transmission. Further improvement is necessary if a mode purity of 20 db is to be achieved, but the observed results seem reasonable for a first attempt. The problem is apparently one of developing more precise fabrication techniques.

The forward attenuation peaks, or spikes, shown in Fig. 2 for 0.035-inch and 0.045-inch wall thicknesses, are attributed either to unwanted mode conversion or to possible higher order TE_{0n} modes. The fact that these peaks tended to shift outside the band of interest as the wall thickness was increased is considered to be of some importance. However, it was felt that adequate evaluation of the test data required a better understanding of the nature of the TE_{0n} modes propagating in the dielectric-cylinder-loaded waveguide. A theoretical calculation was therefore made of the field distribution in this transmission structure.

IV. TE_{0n} Field Distribution

Boundary Values Solution

A cross section of the dielectric cylinder-loaded waveguide is shown in Fig. 4. The cross section of this waveguide is divided into air-filled regions I and III and the dielectric region II, bounded by the dielectric cylinder radii r_1 and r_2.

Solutions of Maxwell's equations in cylindrical coordinates result in the following longitudinal magnetic field expressions [7]:

$$\text{region I,}\quad Hz_1 = A_1J_0(k_1r) + B_1N_0(k_1r) \qquad k_1 \neq 0 \tag{2}$$

$$\text{region II,}\quad Hz_2 = A_2J_0(k_2r) + B_2N_0(k_2r) \qquad k_2 \neq 0 \tag{3}$$

$$\text{region III,}\quad Hz_3 = A_3J_0(k_1r), \tag{4}$$

where $J_0(kr)$ is the zero-order Bessel function of argument kr and $N_0(kr)$ is the zero-order Neumann function of the same argument.

The circumferential electric field in each region is found from

$$E\phi = \frac{j\omega\mu\epsilon}{k_c^2}\frac{\partial Hz}{\partial r}. \tag{5}$$

All of the above fields have a propagation factor $e^{j(\omega t-\beta z)}$ which has been omitted to simplify the notation.

The relationship between the cutoff wave numbers k_1 and k_2 and the propagation constant $\beta=\omega/v_p$ is given by

$$\left.\begin{aligned}\beta^2 &= \omega^2\mu_0\epsilon_0 - k_1^2\\ &= \epsilon\omega^2\mu_0\epsilon_0 - k_2^2\end{aligned}\right\}, \tag{6}$$

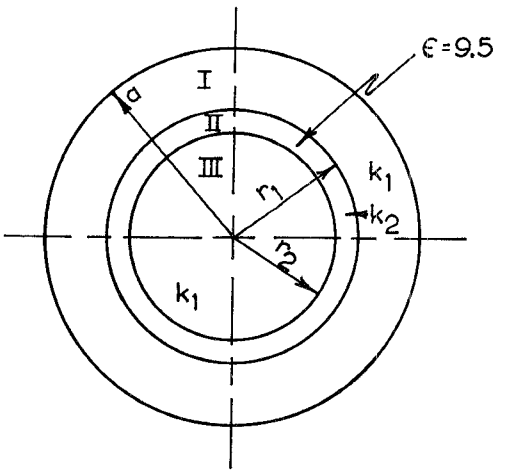

Fig. 4—Cross section of waveguide containing concentric dielectric cylinder.

where, as before, $\omega\sqrt{\mu_0\epsilon_0}=2\pi/\lambda_0=k_0$, the free space propagation constant. The relation between k_1 and k_2 obtained from (6) is

$$k_2^2 - k_1^2 = (\epsilon - 1)k_0^2. \tag{7}$$

Note that when $0<k_1^2<k_0^2$, $\beta^2<k_0^2$ and the phase velocity of propagation v_p is greater than the velocity of light. On the other hand, when $\epsilon k_0^2-k_2^2>k_0^2$, the phase velocity is less than the velocity of light and there exists what might be called a "slow-wave" mode of propagation. The latter case requires $k_1^2<0$ and leads to fields in the air-filled regions which decay as a function of the radial distance away from the dielectric cylinder. In all cases, the field solutions in the three regions must satisfy the boundary matching conditions

$$E\phi_1 = 0 \qquad \text{at } r = a \tag{8}$$

$$\left.\begin{aligned}E\phi_1 &= E\phi_2\\ Hz_1 &= Hz_2\end{aligned}\right\} r = r_1 \tag{9a}$$

$$\left.\begin{aligned}E\phi_2 &= E\phi_3\\ Hz_2 &= Hz_3\end{aligned}\right\} r = r_2 \tag{9b}$$

$$E\phi_3 = 0 \qquad \text{at } r = 0. \tag{10}$$

Relation (10) is satisfied in region III by choosing the longitudinal magnetic field representation of (4).

Details of the field solutions are given in Appendix II. A general form for the characteristic equation obtained from the matching conditions (9a) and (9b) is

$$\frac{E\phi_3(k_1r_2)}{Hz_3(k_1r_2)} = \frac{j\omega\mu_0}{k_2}\,ct(k_2r_2, k_2r_1) \cdot \left\{\frac{Tn(k_2r_1, k_2r_2) - \dfrac{k_2}{j\omega\mu_0}\dfrac{E\phi_1(k_1r_1)}{Hz_1(k_1r_1)}}{ct(k_2r_1, k_2r_2) + \dfrac{k_2}{j\omega\mu_0}\dfrac{E\phi_1(k_1r_1)}{Hz_1(k_1r_1)}}\right\}, \tag{11}$$

where the functions $ct(k_2r_2,\ k_2r_1)$, $ct(k_2r_1,\ k_2r_2)$ and $Tn(k_2r_1,\ k_2r_2)$ are radial cotangent and tangent functions defined, plotted and tabulated by Marcuvitz [8]. The form of the field solutions in the air-filled regions I and III is dependent on whether a "fast-wave" or a "slow-wave" case is under consideration. For the "fast-wave" case we must have, using (7),

$$0 < k_1^2 < k_0^2$$
$$(\epsilon - 1)k_0^2 < k_2^2 < \epsilon k_0^2. \tag{12}$$

From (12) we see that if $\epsilon \gg 1$, k_2 is relatively constant for all "fast-wave" solutions.

The ratios E/H in (11) may be written for the "fast-wave" case as

$$\frac{E\phi_1(k_1r_1)}{Hz_1(k_1r_1)} = \frac{j\omega\mu_0}{k_1}\, Tn(k_1r_1,\ k_1a) \tag{13}$$

$$\frac{E\phi_3(k_1r_2)}{Hz_3(k_1r_2)} = \frac{-j\omega\mu_0}{k_1}\,\frac{J_1(k_1r_2)}{J_0(k_1r_2)}\,. \tag{14}$$

For the "slow-wave" case we have $k_1^2<0$, the relation (7) yielding the limits

$$-(\epsilon - 1)k_0^2 < k_1^2 < 0$$
$$0 < k_2^2 < (\epsilon - 1)k_0^2. \tag{15}$$

We also find

$$\frac{E\phi_1(k_1r_1)}{Hz_1(k_1r_1)} = \frac{j\omega\mu_0}{k_1}\,\frac{Q}{P} \tag{16}$$

$$\frac{E\phi_3(k_1r_2)}{Hz_3(k_1r_2)} = \frac{-j\omega\mu_0}{k_1}\,\frac{I_1(k_1r_2)}{I_0(k_1r_2)}, \tag{17}$$

where, from the field expressions in Appendix II,

$$\frac{Q}{P} = \frac{\left(\frac{K_1(k_1r_1)}{K_0(k_1r_1)}\right) - \left(\frac{I_1(k_1r_1)}{I_1(k_1a)}\right)\left(\frac{K_1(k_1a)}{K_0(k_1r_1)}\right)}{1 + \left(\frac{I_0(k_1r_1)}{I_1(k_1a)}\right)\left(\frac{K_1(k_1a)}{K_0(k_1r_1)}\right)}\,. \tag{18}$$

The functions $I_0(k_1r_2)$, $I_1(k_1r_2)$ are related to the zero- and first-order Bessel functions of imaginary argument, while $K_0(k_1r)$ and $K_1(k_1r)$ are related to the zero- and first-order Hankel functions of the first kind having imaginary arguments.

The ellipticity of the RF magnetic field at the dielectric boundaries r_1, r_2 may be expressed in terms of the ratio of the field components. We have the general relation

$$H_r = \frac{\beta}{\omega\mu_0}\, E\phi. \tag{19}$$

Hence the ellipticity ratio at $r=r_1$ is given by

$$R_1 = \frac{Hr_1(k_1r_1)}{Hz_1(k_1r_1)} = -\frac{\beta}{\omega\mu_0}\,\frac{E\phi_1(k_1r_1)}{Hz_1(k_1r_1)}, \tag{20}$$

and at $r=r_2$,

$$R_2 = \frac{Hr_3(k_1r_2)}{Hz_3(k_1r_2)} = -\frac{\beta}{\omega\mu_0}\,\frac{E\phi_3(k_1r_2)}{Hz_3(k_1r_2)}\,. \tag{21}$$

For the "fast-wave" case we have,

$$R_1 = -j\frac{\beta}{k_1}\, Tn(k_1r_1,\ k_1a) \tag{22}$$

$$R_2 = j\frac{\beta}{k_1}\,\frac{J_1(k_1r_2)}{J_0(k_1r_2)}\,. \tag{23}$$

The "slow-wave" solution yields

$$R_1 = -j\frac{\beta}{k_1}\left|\frac{Q}{P}\right| \tag{24}$$

$$R_2 = j\frac{\beta}{k_1}\,\frac{I_1(k_1r_2)}{I_0(k_1r_2)}\,. \tag{25}$$

For the "fast-wave" condition $k_1^2>0$, one may determine k_1 as a function of r_1 and r_2 by solving the characteristic equation (11) [substituting (13) and (14) with condition (12)] simultaneously with (6). Obviously when $r_1=r_2$, $k_1=3.8317/a$. However, as the wall thickness r_1-r_2 increases from zero, one would intuitively expect that there must be a corresponding decrease in k_1^2. At some point the solutions should change to those for the "slow-wave" condition, where $k_1^2<0$. As the thickness is increased further, the slow-wave condition should hold and $|k_1|^2$ should increase. One may determine $|k_1|$ as a function of r_1 and r_2 when $k_1^2<0$ by substituting (16) and (17) into (11) and solving (11) simultaneously with (6), using the limiting condition (15).

The modes described thus far appear to be the basic TE_{01} fast- and slow-wave modes. As the wall thickness r_1-r_2 increases, one might expect to find higher order "fast-wave" and "slow-wave" solutions. It is possible that these higher order modes could occur at thicknesses for which the TE_{01} slow-wave mode also exists.

From an isolator design standpoint, it is desirable that the ellipticity at the dielectric boundary should have unit magnitude. To achieve this over a reasonable bandwidth, the ellipticity ratios should have the functional behavior given by expressions (24) and (25) so that propagation is in the "slow-wave" mode ($k_1^2<0$). Furthermore, $|k_1|$ should be large. This is seen from the following considerations.

The limiting conditions (15) indicate that $|k_1|$ may be fairly large if the dielectric constant is large.[3] Hence, both $|k_1r_2|$ and $|k_1(a-r_1)|$ may be large. Asymptotic expansion of the ratio $|Q/P|$ indicates that this function has essentially unit magnitude for large argument. The ratio $I_1(k_1r_2)/I_0(k_1r_2)$ also approaches unity. The ratio $\beta/|k_1|$ in (24) and (25), for $k_1^2\approx(\epsilon-1)k_0^2$ and k_2^2 very small, will be seen from (6) to approach $\sqrt{\epsilon/\epsilon-1}$, which

[3] For any practical values of r_1, r_2, and a.

is approximately unity if $\epsilon \gg 1$. Thus, all factors in the ellipticity ratios (24) and (25) have magnitudes approaching unity when $|k_1|^2$ is large.

Although $|k_1^2|$ may change as a function of frequency and wall thickness, the ellipticities defined by (24) and (25) should be insensitive to these changes because of this tendency to approach a definite limit for large $|k_1|$. This is the condition described in Section II in connection with isolator broadbanding. The "fast-wave" mode ellipticities (22) and (23) ($k_1^2 > 0$) do not approach a limit for large $|k_1|$, and should be sensitive functions of both frequency and wall thickness.

V. Numerical Computation

In order to check the preceding theory, specific ring dimensions were chosen and an attempt was made to find a solution of the characteristic equation at 35 Gc. The dimensions chosen were those of a dielectric ring combination used in one of the experimental isolator configurations of Fig. 1, having $r_1 = 0.109$ inch and $r_2 = 0.154$ inch. The dielectric permittivity of the high purity alumina ceramic material from which the rings were constructed was taken to be $\epsilon = 9.5$. Values of the radial tangent and cotangent functions were obtained from curves and tabulations in Marcuvitz [8]. A "slow-wave" solution of the characteristic equation was found, hand computation indicating that for the above values of r_1 and r_2, $k_1^2 \approx -1/2(\epsilon - 1)k_0^2$.

The ellipticity at the boundaries r_1 and r_2 was computed from (24) and (25) using (6) and the limits indicated by (15). These are plotted in Fig. 5 as a function of the normalized cutoff constant, $p = |k_1| / \sqrt{(\epsilon - 1)} k_0$. It will be noted that at the inner boundary $r_2 = 0.109$ inch, the ellipticity ratio is approximately unity for all values of p.

Small argument limits were obtained by substituting for the I and K functions in (24) and (25) their small argument approximations. For $|k_1| \ll 1$,

$$R_1 \approx jk_0\left(\frac{a^2}{r_1} - r_1\right) + \text{terms of order } |k_1| \text{ and } |k_1|^2(\ln |k_1|) + \text{higher order terms} \tag{26a}$$

$$R_2 \approx -j\frac{k_0 r_2}{2} + \text{terms of order } |k_1| + \text{higher order terms.} \tag{26b}$$

If the terms involving $|k_1|$ are neglected and if $r_2 = \lambda_0/\pi$, it is apparent from (26b) that the magnitude of R_2 should approach unity. From (26a), R_1 should have a magnitude approaching unity if $k_0 r_1 = \sqrt{1 + k_0^2 a^2} - 1$. Numerical computation using (26b) at a frequency of 35 Gc indicates that if R_2 is to have unit magnitude for small values of $|k_1|$, we should indeed find r_2 to be 0.109 inch. Similarly, an outer radius for which the magnitude of R_1 should approach unity when $|k_1|$ is small is $r_1 = 0.263$ inch.

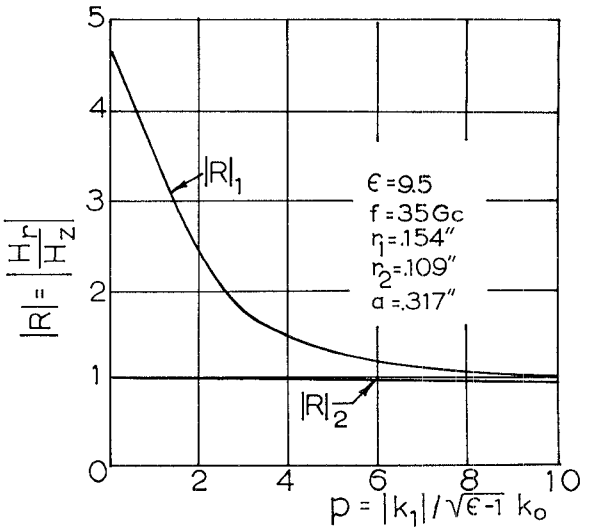

Fig. 5—H_r/H_z as a function of normalized cutoff constant, at the inner and outer boundaries of a ceramic cylinder with ID 0.218 inch, OD 0.308 inch.

The numerical results in the preceding paragraph and in Fig. 5 indicate that the experimental configurations of Fig. 1 should tend to have unit magnetic field ellipticity at the inner boundary $r_2 = 0.109$ inch, and that significant nonreciprocal attenuation therefore should indeed have been obtained. They also tend to support the data in Fig. 2. The computations have additional significance in connection with the design of isolators for maximum bandwidth.

Intuitively, one expects "slow-wave" solutions of the characteristic equation to be such that, for given r_1 and r_2, $|k_1|$ satisfying (11) has a direct relationship to the wavelength. At low frequencies the wall thickness is a small fraction of a wavelength and the fields in the air regions decay slowly as a function of the radial distance from the dielectric. The field expressions are such that for this to occur $|k_1|$ must be small. At high frequencies the wall thickness becomes a large fraction of a wavelength and energy tends to concentrate in the dielectric. When this occurs, the fields in the air region decay rapidly and $|k_1|$ is large. If extreme bandwidth is desired, one might use either (26a) or (26b) to calculate a bounding radius for which almost circular polarization should exist at the lowest frequency in the band of interest, where $|k_1|$ is a minimum. At higher frequencies $|k_1|$ should increase, and the magnitude of the ellipticity should approach a limit of unity because of the nature of the defining functions (24) and (25). Choice of the ring wall thickness is influenced by the desired bandwidth. However, it is also influenced by energy concentration factors which have not been considered here.

VI. Conclusions

Experimental data indicate that appreciable nonreciprocal attenuation may be obtained from isolator

configurations of the type described in Section III. Analytical consideration of the boundary value problem of a dielectric ring mounted concentrically in a waveguide propagating the TE_{01} mode has yielded expressions for magnetic field ellipticities at the ring boundaries which tend to support the experimental data.

Appendix I

Experimental Measurement Techniques

Exact measurement of attenuation and mode purity in TE_{01} mode circular waveguide is extremely difficult. However, reasonable indications of the attenuation may be obtained by a fairly simple, but approximate, procedure which utilizes a TE_{10} rectangular waveguide power detector coupled to the circular waveguide through a small coupling hole. The rectangular waveguide must be oriented so that its broad walls are parallel to the circular waveguide axis, thus insuring that coupling is to Hz in the circular guide. The circular guide beyond the coupling hole is terminated in a matched load. If only the TE_{01} mode is present, power coupled to the output waveguide detector is independent of the angular location of the coupling hole. However, if mode impurities are present, the output power will be a function of angular position since the longitudinal magnetic field components of these modes are functions of the circular waveguide angular coordinates. The output signal will also be a function of the relative phases of the various modes, which are functions of the distance of the coupling hole from the point at which the impurities are generated.

The measuring procedure used to obtain the data of Figs. 2 and 3 was one in which the output power detector was attached by a rotating connection to the output of a length of circular waveguide which was to serve as the "test fixture." An average power output from the empty test section was obtained by averaging the maximum and minimum levels noted as the detecting element was rotated through an angle of 360°. Care was taken to use reasonably perfect waveguide, and radial vane [9] mode filters were used near suspected discontinuities and immediately in front of the detector coupling hole. However, there was generally a residual angular variation in power level of the order of a decibel corresponding to a TE_{11} (most pessimistic) mode impurity roughly 20 db below the desired mode.

Isolator configurations were measured by inserting them in the test waveguide and averaging the maximum and minimum output power levels as the detector was rotated through an angle of 360°. The difference in average power level measured with and without the attenuating element in the waveguide served as an indication of the attenuation in the ferrite element.

For isolators having appreciable reverse attenuation, the angular variation in the reverse direction sometimes became quite large. The reason for this result is clearly the fact that the TE_{01} mode was attenuated, reducing the nonvarying component of Hz. On the other hand, unwanted modes were transmitted with little or no attenuation, so that their relative amplitudes become larger when compared with the amplitude of the attenuated mode. For this reason it was sometimes necessary to average power levels which might vary between, say 12 and 18 db giving an average reading of 15 db. However, if this variation was reduced, say, from 6 db to 3 db, by additional filtering, the average level still remained at about 15 db. When the preceding measuring technique is used, highest measurement accuracy should be obtained for angular variations which are small compared to the magnitude of the average attenuation being measured. Thus, forward attenuation measurement accuracy will be greatest when the angular variation in output power is minimized. Larger attenuation swings should be tolerable in the direction of reverse attenuation because the reverse attenuation is generally higher.

Appendix II

Derivation of Field Expressions and Characteristic Equation

From the basic expressions for longitudinal magnetic field (2), (3), (4), and the relation (5), we may write for the fields in region I,

$$Hz_1 = A_1 J_0(k_1 r) + B_1 N_0(k_1 r) \tag{27}$$

$$E\phi_1 = \frac{-j\omega\mu_0}{k_1}\left[A_1 J_1(k_1 r) + B_1 N_1(k_1 r)\right]. \tag{28}$$

The boundary condition (8) requires that $A_1 J_1(k_1 a) = -B_1 N_1(k_1 a)$, yielding final expressions for the fields in region I,

$$Hz_1 = \frac{A_1}{N_1(k_1 a)}\left[J_0(k_1 r)N_1(k_1 a) - N_0(k_1 r)J_1(k_1 a)\right] \tag{29}$$

$$E\phi_1 = \frac{j\omega\mu_0}{k_1}\,\frac{A_1}{N_1(k_1 a)}\left[J_1(k_1 r)N_1(k_1 a) - N_1(k_1 r)J_1(k_1 a)\right]. \tag{30}$$

Although these solutions are not valid at $k_1 = 0$, they approach a finite limit for small values of k_1. The ratio $E\phi_1/Hz_1$ may be expressed in terms of the large radial tangent function defined and tabulated in Marcuvitz [8], as indicated in (13).

The fields in region II may be written,

$$Hz_2 = A_2 J_0(k_2 r) + B_2 N_0(k_2 r) \tag{31}$$

$$E\phi_2 = \frac{-j\omega\mu_0}{k_2}\left[A_2 J_1(k_2 r) + B_2 N_1(k_2 r)\right]. \tag{32}$$

The matching condition (9a) results in the following solutions for the constants:

$$A_2 = \left(\frac{\pi k_2 r_1}{2}\right) \cdot \left[\frac{-k_2}{j\omega\mu_0} E\phi_1(k_1r_1)N_0(k_2r_1) - Hz_1(k_1r_1)N_1(k_2r_1)\right] \quad (33)$$

$$B_2 = \left(\frac{\pi k_2 r_1}{2}\right) \cdot \left[\frac{k_2}{j\omega\mu_0} E\phi_1(k_1r_1)J_0(k_2r_1) + Hz_1(k_1r_1)J_1(k_2r_1)\right]. \quad (34)$$

Then,

$$Hz_2 = \left(\frac{\pi k_2 r_1}{2}\right)\left\{Hz_1(k_1r_1)[J_1(k_2r_1)N_0(k_2r) - N_1(k_2r_1)J_0(k_2r)] + \frac{k_2}{j\omega\mu_0} E\phi_1(k_1r_1)[J_0(k_2r_1)N_0(k_2r) - N_0(k_2r_1)J_0(k_2r)]\right\} \quad (35)$$

$$E_2 = \frac{-j\omega\mu_0}{k_2}\left(\frac{\pi k_2 r_1}{2}\right)\left\{Hz_1(k_1r_1)[J_1(k_2r_1)N_1(k_2r) - N_1(k_2r_1)J_1(k_2r)] - \frac{k_2}{j\omega\mu_0} E\phi_1(k_1r_1)[N_0(k_2r_1)J_1(k_2r) - J_0(k_2r_1)N_1(k_2r)]\right\}. \quad (36)$$

The matching condition (9b) leads to the characteristic equation

$$\frac{E\phi_3(k_1r_2)}{Hz_3(k_1r_2)} = \frac{j\omega\mu_0}{k_2} f_1(k_2r_2, k_2r_1) \cdot \left\{\frac{g(k_2r_1, k_2r_2) - \frac{k_2}{j\omega\mu_0}\frac{E\phi_1(k_1r_1)}{Hz_1(k_1r_1)}}{f_2(k_2r_1, k_2r_2) + \frac{k_2}{j\omega\mu_0}\frac{E\phi_1(k_1r_1)}{Hz_1(k_1r_1)}}\right\}, \quad (37)$$

where

$$f_1(k_2r_2, k_2r_1) = -\frac{[N_0(k_2r_1)J_1(k_2r_2) - J_0(k_2r_1)N_1(k_2r_2)]}{[J_0(k_2r_1)N_0(k_2r_2) - N_0(k_2r_1)J_0(k_2r_2)]}, \quad (38)$$

which is immediately identified in Marcuvitz [8] as $ct(k_2r_2, k_2r_1)$.

The function

$$g(k_2r_1, k_2r_2) = \frac{[J_1(k_2r_1)N_1(k_2r_2) - N_1(k_2r_1)J_1(k_2r_2)]}{[N_0(k_2r_1)J_1(k_2r_2) - J_0(k_2r_1)N_1(k_2r_2)]} \quad (39)$$

may be identified as $Tn(k_2r_1, k_2r_2)$.

Finally,

$$f_2(k_2r_1, k_2r_2) = \frac{[J_1(k_2r_1)N_0(k_2r_2) - N_1(k_2r_1)J_0(k_2r_2)]}{[J_0(k_2r_1)N_0(k_2r_2) - N_0(k_2r_1)J_0(k_2r_2)]}, \quad (40)$$

which may be identified as the function $ct(k_2r_1, k_2r_2)$.

The fields in region III become

$$Hz_3 = A_3J_0(k_1r) \quad (41)$$

$$E\phi_3 = \frac{-j\omega\mu_0}{k_1} A_3J_1(k_1r), \quad (42)$$

where A_3 may be obtained from the matching conditions (9b), leading to the characteristic equation (37).

When $k_1^2 < 0$, the fields in regions I and III become functions of imaginary argument. The Bessel functions of imaginary argument are defined and tabulated, and the fields in region III can be immediately written in terms of these functions by substituting jk_1 for k_1 in (41) and (42). We then obtain

$$Hz_3 = A_3I_0(k_1r) \quad (43)$$

$$E\phi_3 = \frac{-j\omega\mu_0}{k_1} A_3I_1(k_1r). \quad (44)$$

The fields in region I must, however, be re-expressed in terms of Bessel functions and Hankel functions of the first kind, since the latter function is defined and tabulated for imaginary argument but the Neumann function is not. When this is done and jk_1 is substituted for k_1 in (29) and (30), the field solutions in region I become

$$Hz_1 = \frac{(A_1 + jB_1)}{K_1(k_1a)}[I_0(k_1r)K_1(k_1a) + K_0(k_1r)I_1(k_1a)] = \frac{(A_1 + jB_1)}{K_1(k_1a)} P(k_1r, k_1a), \quad (45)$$

and

$$E\phi_1 = \frac{j\omega\mu_0}{k_1}\frac{(A_1 + jB_1)}{K_1(k_1a)} \cdot [K_1(k_1r)I_1(k_1a) - I_1(k_1r)K_1(k_1a)] = \frac{j\omega\mu_0}{k_1}\frac{(A_1 + jB_1)}{K_1(k_1a)} Q(k_1r, k_1a). \quad (46)$$

Definitions of the I and K functions are given in Ramo and Whinnery [7]. The definitions include multiplicative constants which ensure that these functions are always real.

ACKNOWLEDGMENT

The author wishes to thank Melabs consultants Drs. B. A. Auld and J. H. Burgess for many helpful discussions. He also wishes to acknowledge contributions of S. S. Shapiro toward the basic design, in the development of measuring techniques and during early phases of the work described in paragraph 2 of Section III. The experimental measurements were made by C. Fulker and K. Yamaguchi. J. Green and members of the Melabs model shop developed techniques used in the fabrication of experimental devices. C. D. Neudorfer of USAERDL reviewed the original draft of this paper and made a number of suggestions which greatly added to the clarity of the presentation.

Finally, the author wishes to thank Dr. I. H. Solt, Jr. and Fairchild Semiconductor Lab., Palo Alto, Calif. for help during the preparation of this paper.

REFERENCES

[1] A. G. Fox, S. E. Miller, and M. T. Weiss, "Behavior and application of ferrites in the microwave region," *Bell Sys. Tech. J.*, vol. 34, pp. 5–103; January, 1955.
[2] B. Lax and K. Button, "Microwave Ferrites and Ferrimagnetics," McGraw-Hill Book Co., Inc., New York, N. Y.; 1962.
[3] P. H. Vartanian, W. P. Ayres, and A. L. Helgesson, "Propagation in dielectric slab loaded rectangular waveguide," IRE TRANS. ON MICROWAVE THEORY AND TECHNIQUES, vol. MTT-6, pp. 215–222; April, 1958.
[4] R. F. Soohoo, "Theory and Applications of Ferrites," Prentice. Hall, Inc., Englewood Cliffs, N. J., p. 187; 1960.
[5] R. A. Henschke, D. A. Parkes, and S. S. Shapiro, "Ferrite Devices for Receiving Systems," Melabs, Palo Alto, Calif., Final Rept., Contract No. DA36-039 SC-85296; February, 1960–August, 1961.
[6] R. A. Henschke, "Ferrite Devices for Receiving Systems," Melabs, Palo Alto, Calif., First Quarterly Rept., Contract No. DA36-039 SC-88949, p. 16; February 15, 1962–May 14, 1962.
[7] S. Ramo and J. R. Whinnery, "Fields and waves in Modern Radio," John Wiley and Sons, Inc., New York, N. Y., 2nd ed.; 1953. See especially p. 165.
[8] N. Marcuvitz, "Waveguide Handbook," McGraw-Hill Book Co., Inc., New York, N. Y.; 1951.
[9] S. E. Miller and A. C. Beck, "Low-loss waveguide transmission," PROC. IRE, vol. 41, pp. 348–358; March, 1953.

Modes in Coupled Optical Resonators with Active Media

J. R. FONTANA, MEMBER, IEEE

Summary—**A general method is proposed to analyze the properties of optical systems composed of several coupled resonators. It is shown that by using appropriate matrices to represent the fields in the resonators and the couplings between them, an equation can be written, often by inspection, for the eigenvalue $s=\sigma+j\omega$ which gives the frequency and the rate of growth of the fields for all the modes of a given system.**

A re-entrant coupled system with loss and gain regions is discussed as an example. The effects of changes in mirror transmission, resonator length and medium properties are studied using the method.

I. INTRODUCTION

IT HAS BEEN suggested by various authors[1,2] that optical masers with desirable properties could be obtained by operating the active medium in a system of coupled optical resonators rather than in simple structures of the Fabry-Perot type. In the latter many modes of oscillation are allowed, separated by equal frequency intervals and with relative growth rates which depend only on the active medium and not on the resonator. Simultaneous oscillation in several modes is thus possible within the linewidth of usual materials. Coupled systems can have modes with unevenly spaced frequencies and different rates of growth or of attenuation if lossy materials are used as well as active media. These properties depend on the resonant system as well as the materials, and are determined by mechanical design and adjustment. Possible features include selective mode suppression, so that only one mode oscillates, or so that only two oscillate with controllable frequency separation.

The properties of arbitrary coupled resonator systems can be studied as an eigenvalue problem. The time-dependence properties of each mode are given by the complex exponential exp (st), where $s=\sigma+j\omega$ expresses the frequency of oscillation and the rate of growth or decay of the mode. The form of the eigenvalue equation specifies the freedom one has to choose the eigenvalues s; that is, it shows the possibilities and limitations of each particular system and also of coupled systems in general. The analysis is greatly simplified by considering that the traveling waves inside the resonators are approximately TEM. Use can thus be made of equivalent circuits with coupled TEM transmission lines.

II. TWO-MIRROR RESONATORS

To introduce the method proposed, we consider first a simple, uncoupled system. Fig. 1(a) shows a resonator formed by two identical mirrors in a medium assumed

Manuscript received February 12, 1964; revised March 16, 1964.
The author is with the Department of Electrical Engineering, University of Minnesota, Minneapolis, Minn.

[1] D. A. Kleinman and P. Kisliuk, "Discrimination against unwanted orders in the Fabry-Perot resonator," *Bell Sys. Tech. J.*, vol. 41, p. 453; 1962.
[2] M. Birnbaum and T. L. Stocker, "Mode selection properties of segmented rod lasers," *J. Appl. Phys.*, vol. 34, p. 3414; 1963.